geologica acta

Citation: Tomás, S., Parcerisa, D., Cantarero, I., Baqués, V., Salas, R., Travé, A., 2025. Linking early diagenesis and relative sea-level changes in ancient corals: a multiproxy approach from the Benassal Formation (Lower Cretaceous, Maestrat Basin, E Spain. Geologica Acta, 23.19, 1-18. DOI: 10.1344/GeologicaActa2025.23.19

Online ISSN: 1696-5728

Linking early diagenesis and relative sea-level changes in ancient corals: a multiproxy approach from the Benassal Formation (Lower Cretaceous, Maestrat Basin, E Spain)

Sara Tomás[1] David Parcerisa[2] Irene Cantarero[3] Vinyet Baqués[3] Ramon Salas[3] Anna Travé[3]

[1]Departament de Geologia, Facultat de Ciències, Universitat Autònoma de Barcelona (UAB)
c/ de la Vall Moronta s/n. 08193 Bellaterra, Barcelona, Spain. Tomás Email: sara.tomas.lafaja@uab.cat

[2]Departament d´Enginyeria Minera, Industrial i TIC, Universitat Politècnica de Catalunya (UPC)
Avinguda Bases de Manresa, 61-73, 08242, Manresa, Spain. Parcerisa Email: david.parcerisa@upc.edu

[3]Departament de Mineralogia, Petrologia i Geologia Aplicada, Facultat de Ciències de la Terra, Universitat de Barcelona (UB)
c/ Martí i Franquès s/n. 08028 Barcelona, Spain. Cantarero Email: i_cantarero@ub.edu;
Baqués Email: vbaqués@ub.edu; Salas Email: ramonsalas@ub.edu; Travé Email: atrave@ub.edu

ABSTRACT

The Aptian shallow-water carbonate platform of the Benassal Formation in eastern Spain (Maestrat Basin) contains facies dominated by scleractinian corals. Corals and coral reefs are widely used as environmental archives; however, the effects of their complex diagenetic evolution are a major factor impacting reliable reconstructions of the environments. This study addresses the environmental signatures (i.e. relative sea-level changes) and burial conditions that controlled the various diagenetic minerals present in the Aptian coral facies. A multiproxy approach including petrographic and geochemical evaluation reveals the diagenetic pathways, fluid compositions and timing accounting for the syn- to post-depositional history of this ancient coral facies. Cc1, which shows low Fe and Mn content and high Na content, precipitated within the primary porosity, alongside the replacement of coral skeletons, in a mixing zone dominated by marine waters. Cement Cc2, characterized by its higher Fe and Mn content and low Na values, precipitated in the mixing zone dominated by meteoric waters related to a relative sea-level drop. Cement Cc3, distinguished by low Fe and Mn content and high Na content, reflects a subsequent phase of increased marine influence, likely associated with a relative sea-level rise. Silica and isolated rhombohedral dolomite crystals formed concurrently in this mixing zone. During intermediate burial, saddle dolomite and cement Cc4 precipitated from high-temperature formation brines. Finally, during uplift, meteoric fluids caused the calcitization of previously formed dolomite rhombohedra.

KEYWORDS **Maestrat Basin. Coral facies. Sea-level changes. Diagenesis. Silicification.**

INTRODUCTION

Fossil scleractinian corals easily record the various diagenetic episodes that have undergone from their formation to the present, owing to their high primary porosity and the mineral reactivity of their skeletons. Common diagenetic alterations, such as micritization, neomorphism, replacement, cementation and dissolution result in textural, chemical, and mineralogical changes within their skeletal structures. A wide number of studies highlight the importance of understanding the compositional and geochemical heterogeneities caused

by diagenesis to perform reliable (paleo) environmental reconstructions from corals. (*e.g.* Allison *et al.*, 2007; Enmar *et al.*, 2000; McGregor and Gagan, 2003; Müller *et al.*, 2001; Ribaud-Laurenti *et al.*, 2001; Sayani *et al.*, 2011).

Among the diagenetic processes affecting scleractinian corals, a key transformation is the partial to complete neomorphism of the original aragonite skeleton to calcite. This neomorphic alteration occurs in various diagenetic settings and fluid environments, often involving marine (Badali, 2003; Maliva, 1998; Wilson *et al.*, 2013) and/or meteoric waters (Sherman *et al.*, 1999; Web *et al.*, 2009). Another significant diagenetic process is the precipitation of secondary calcite cements within pore spaces (*e.g.* Friedman *et al.*, 1974; James *et al.*, 1976; Macintyre and Marshall, 1988; Perry and Hepburn, 2008), which can occur at any stage of the coral diagenetic history. Additionally, in coral facies, authigenic calcite is often associated with other minerals such as dolomite and silica, formed through processes of replacement and cementation (Al-Dabbagh and El-Sorogy, 2016; Andrade *et al.*, 2020; El-Saiy and Jordan, 2007; Jacka, 1974).

The Aptian coral facies of the Benassal Formation (Fm.) provide an exceptional opportunity to explore a wide variety of diagenetic processes, including the interplay between various phases of calcite, dolomite, and silica, and the mechanisms (*i.e.* relative sea-level changes, burial conditions) accounting for these processes. To date, only one study (Tomás *et al.*, 2007c) has focused on the diagenetic evolution of these coral facies. This contrasts with the numerous publications addressing the fault-controlled hydrothermal dolostones of the Benassal Fm., which are located just above the coral facies (Centrella *et al.*, 2023; Gomez-Rivas *et al.*, 2012, 2014; Humphrey *et al.*, 2022; Martín-Martín *et al.*, 2012, 2013, 2015, 2018; Yao *et al.*, 2020).

The aim of this paper is to document, for the first time, in detail the diagenetic evolution of the Aptian coral facies of the Benassal Fm. by integrating petrography, elemental geochemistry, and stable isotopic analyses. This study highlights the relevance of using a wide variety of diagenetic minerals to gain a better understanding of the paleoenvironments and burial conditions in which they formed. It establishes the diagenetic pathways, fluid compositions, and timing of the syn- to post-depositional history of these ancient coral facies.

GEOLOGICAL SETTING

The Aptian scleractinian coral facies studied occur in the southeast of the Maestrat Basin, which is located in eastern Spain (Fig. 1). The Maestrat Basin, one of the Mesozoic extensional sub-basins that make up the Iberian Basin, developed during the Late Jurassic-Early Cretaceous rifting phase (Salas and Casas, 1993; Salas *et al.*, 2001) and underwent tectonic inversion during the Alpine Orogeny. Later, during the Neogene, an extensional phase reactivated Mesozoic syn-rift and Alpine contractional structures forming the Valencia Trough and the current Western Mediterranean Basin (Gomez-Rivas *et al.*, 2012; Roca and Guimerà, 1992).

The Benicàssim study area is structurally controlled by the NNE-SSW trending Benicàssim normal fault and the NE-SW trending Juvellús Fault, both of which developed during the Late Jurassic-Early Cretaceous rifting phase, as evidenced by the thick (>2km) Lower Cretaceous sedimentary record (Gomez-Rivas *et al.*, 2012; Martín-Martín *et al.*, 2013). Additionally, major Neogene faults at the eastern part of the area truncate and repeat the Lower Cretaceous succession (Fig. 1A).

During the Aptian, marine conditions prevailed, leading to the development of an over 1000m thick succession of shallow-marine carbonate platforms (ramp-like) in the Maestrat Basin. This succession is well-exposed in the outcrops of El Palasiet (which include the coral-bearing facies of La Venta, object of this study) and Racó de Cantallops, located a few kilometers northeast of Benicàssim urban centre. It belongs to the Benassal Formation, which spans from the terminal early Aptian to the early Albian (Bover-Arnal *et al.*, 2016; Martín-Martín *et al.*, 2013, 2015). The facies and depositional environments of the Benassal Fm. in the area of Benicàssim have been previously studied by Tomás (2007) and Tomás *et al.*, (2007b, 2008). The succession begins with approximately 20m of platform glauconite-rich marls containing brachiopods, overlain by a thick package (~200m) of inner ramp shoal deposits. These deposits consist of bioclastic, peloidal and oolitic grainstones with high-angle planar cross-bedding, alternating with marly intervals (a few meter thick) rich in glauconite and brachiopods. Following, a package a few meters thick of outer ramp orbitolinid wackestones is overlain by approximately 50m of coral-rich facies containing abundant lime mud, interpreted as having developed in middle to outer ramp settings. The coral facies are overlain by 90m of low-energy, inner ramp floatstones containing rudists, gastropods and orbitolinids, followed by 350m of middle and outer ramp deposits, including sponge spicule wackestones, orbitolinid wackestones and coral boundstones. The succession concludes with approximately 230m of inner ramp deposits, consisting of 180m of bioclastic-peloidal packstones and grainstones with occasional low-angle cross beds, overlain by 50m of lagoonal rudist floatstones. Previous sequence-stratigraphic analyses of the study succession of the Benicàssim area by

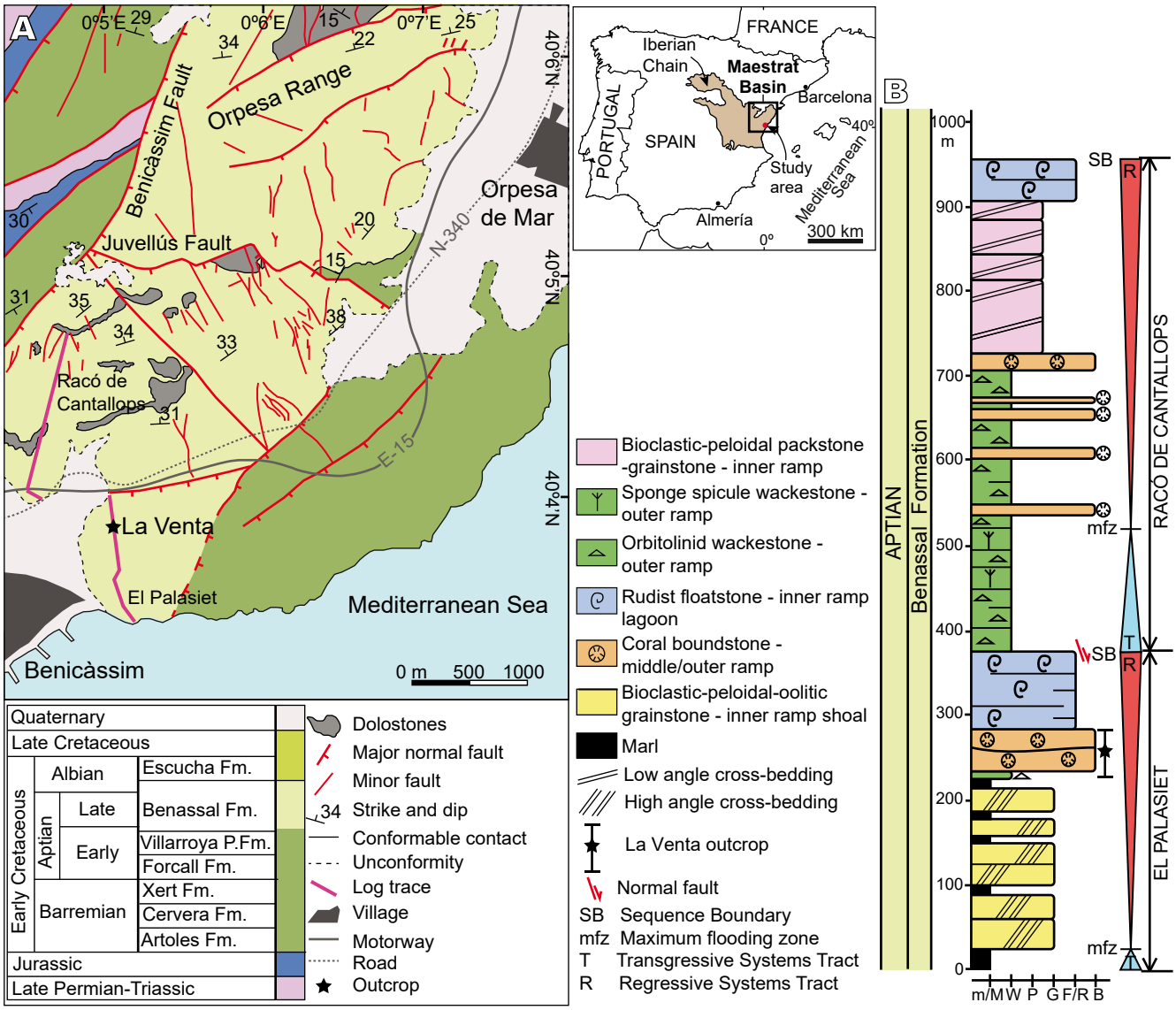

FIGURE 1. A) Geological map of the Benicàssim study area in the eastern Maestrat Basin (eastern Spain). La Venta study outcrop is indicated with a black star. Modified after Martín-Martín *et al.* (2012, 2015). B) Stratigraphy of the Aptian (Cretaceous) of the Benicàssim area. The coral-bearing succession at La Venta is marked with a star.

Martín-Martín *et al.* (2013) have identified two major third-order Transgressive-Regressive (T-R) cycles (Fig. 1B).

METHODS AND ANALYTICAL TECHNIQUES

A total of 300 thin sections were examined with an optical microscope, and about 100 of these were further studied under a Technosyn Cold CathodoLuminescence (CL) microscope (model 8200MkII, operating at 12-17kV with a gun current of 350μA) at the University of Barcelona. Following the petrographic study, a selection of samples was made to analyse their mineralogy, elemental chemistry and stable isotopes. In total, 11 samples were chosen to determine the elemental composition of the different cement types. In this study cements include only skeletal coral parts and associated pore space that were altered. These thin sections were polished and carbon-coated for examination with a CAMECA SX-50 electron microprobe, equipped with four vertically arranged WD X-ray spectrometers at the Centres Científics i Tecnològics de la Universitat de Barcelona (CCiTUB). The operating conditions included an accelerating voltage of 20kV and a beam current of 40nA (for Mn, Fe, Sr, and Na), 20nA (for K, Si and Al), and 6nA (for Ca and Mg) with a spot size of 10µm. The exposure time for each element was set to 10 seconds for all elements analysed in silicates (Na, Mg, Al, Si, K, Ca, and Fe), 30 seconds for minor elements in

carbonates (Na, Mn, Fe and Sr), and 10 seconds for major elements in carbonates (Ca and Mg). Detection limits were 510ppm for Mg, 202ppm for Sr, 158ppm for Na, 194ppm for Al, 236ppm for K, 470ppm for Si, 189ppm for Mn and 218ppm for Fe; these detection limits may represent a limitation of the present study. Analytical totals ranging from 97 to 103% were considered acceptable. For stable isotope analysis, the different types of calcites and dolomites were sampled using a hand micro-drill fitted with bits of 0.2 to 0.5mm in diameter. Silicates and calcite Cc3 were excluded from analysis since were too small to be sampled individually. Care was taken when microdrilling the samples to collect only powder from the micrite and different diagenetic phases, although some samples, especially those of calcites Cc1 and Cc2 may contain a mixture of both carbonate materials, as they were sometimes difficult to separate. Powdered samples were reacted with phosphoric acid under vacuum at 70ºC for 2 minutes. The CO_2 was analysed using an on-line carbonate device connected to a Thermo Finnigan MAT 252 mass spectrometer at the Centres Científics i Tecnològics de la Universitat de Barcelona (CCiTUB) The precision of results was ±0.02‰ for $\delta^{13}C$ and ±0.08‰ for $\delta^{18}O$, with results corrected following standard procedures (Craig and Gordon, 1965) and expressed in ‰ relative to the Vienna (VPDB) standard.

RESULTS

Facies architecture and paleoenvironments of the Aptian coral-dominated facies

The coral-bearing facies at La Venta are characterized by carbonate and marly carbonate beds ranging from decimeter to meter-scale. These facies consist of fine to medium-grained, poorly-sorted wackestones and packstones with abundant lime mud. The main components are scleractinian corals (Fig. 2A-C) that are often encrusted by a thin veneer of red algae and stromatolites (Riding and Tomás, 2006; Tomás *et al.*, 2007a, 2008). Other common components include orbitolinids, sponge tissues, sponge spicules, and bivalves (pectinids and ostreids). Silica selectively replaces the corals, giving them an orange colour (Fig. 2C, D). Less frequently, silica forms elongated nodules (cm-scale) scattered throughout the matrix of the coral facies (Fig. 2E).

The coral facies are classified following the growth fabric nomenclature for fossil scleractinians defined by Insalaco (1998), which is based on the width (w) to height (h) ratio of the dominant coral growth forms. Two main coral fabrics have been differentiated: i) sheetstones, characterized by dish and sheet coral morphologies (Fig. 2A, B) and ii) platestones-domestones, characterized by platy and/or domal forms (Fig. 2A, C). The sheetstones with high w/h ratios are, adapted to low light and interpreted as having developed in distal outer ramp settings; the abundance of sponge spicules in the matrix supports this interpretation. The platestones-domestones with low w/h ratios, are likely indicative of more proximal settings, probably in the middle ramp.

The two types of coral growth fabrics alternate at La Venta outcrop, forming higher-order cycles or parasequences within the regressive hemicycle of the first major T-R depositional sequence (Fig. 1B). Each parasequence shows a shallowing-upward trend, starting with the coral sheetstones and, in some areas, orbitolinid wackestones facies, followed by coral platestones-domestones facies (Fig. 2A).

Petrography of the micrite and diagenetic products of the coral-dominated facies

The coral-dominated facies contain several syn-depositional and diagenetic products, including micrite, neomorphic calcite, calcite cement, dolomite and silica. All products have been analysed in detail under the optical and CL microscope, and their characteristics are described below and illustrated in Figures 3, 4 and 5.

Micrite and peloidal matrix

The carbonate matrix of the coral-dominated wackestone-packstone consists of fine-grained, poorly sorted particulate micrite with scattered bioclasts and other sand-sized particles, thus detrital in origin (Figs. 2B; 3A-B). In contrast, the intra-skeletal cavities of the corals are filled with either dense, homogeneous micrite or peloidal aggregates containing a few allochthonous grains (*e.g.* bioclasts) (Fig. 4A, B). The peloidal fabric mainly comprise micropeloids (<60mm in diameter) within a fenestral microspar matrix. In this study, fenestrae refer to voids filled with carbonate cements in microbialites (see Riding 2011; Summer 1997, 2000 and references therein). Locally, geopetal infills have been observed in intra-skeletal pore spaces, with a dense micrite and peloidal matrix at the base and drusy calcite cement at the top. Additionally, dense micrite also forms thin, isopachous linings (a few microns thick) that coat the surfaces of coral intra-skeletal pore spaces (Fig. 4C, D) and, less commonly, the outer surface of the skeletons. The textural characteristics and/or grading of the micrite and peloidal matrix suggest that they are microbially induced precipitates rather than depositional sediment (for further discussion see Riding and Tomás, 2006). The micritic lining moulding and preserving original coral skeletal structures, is a phenomenon commonly observed in scleractinian corals that is interpreted as result of algal micritization (Bathurst, 1975; Pingitore, 1976).

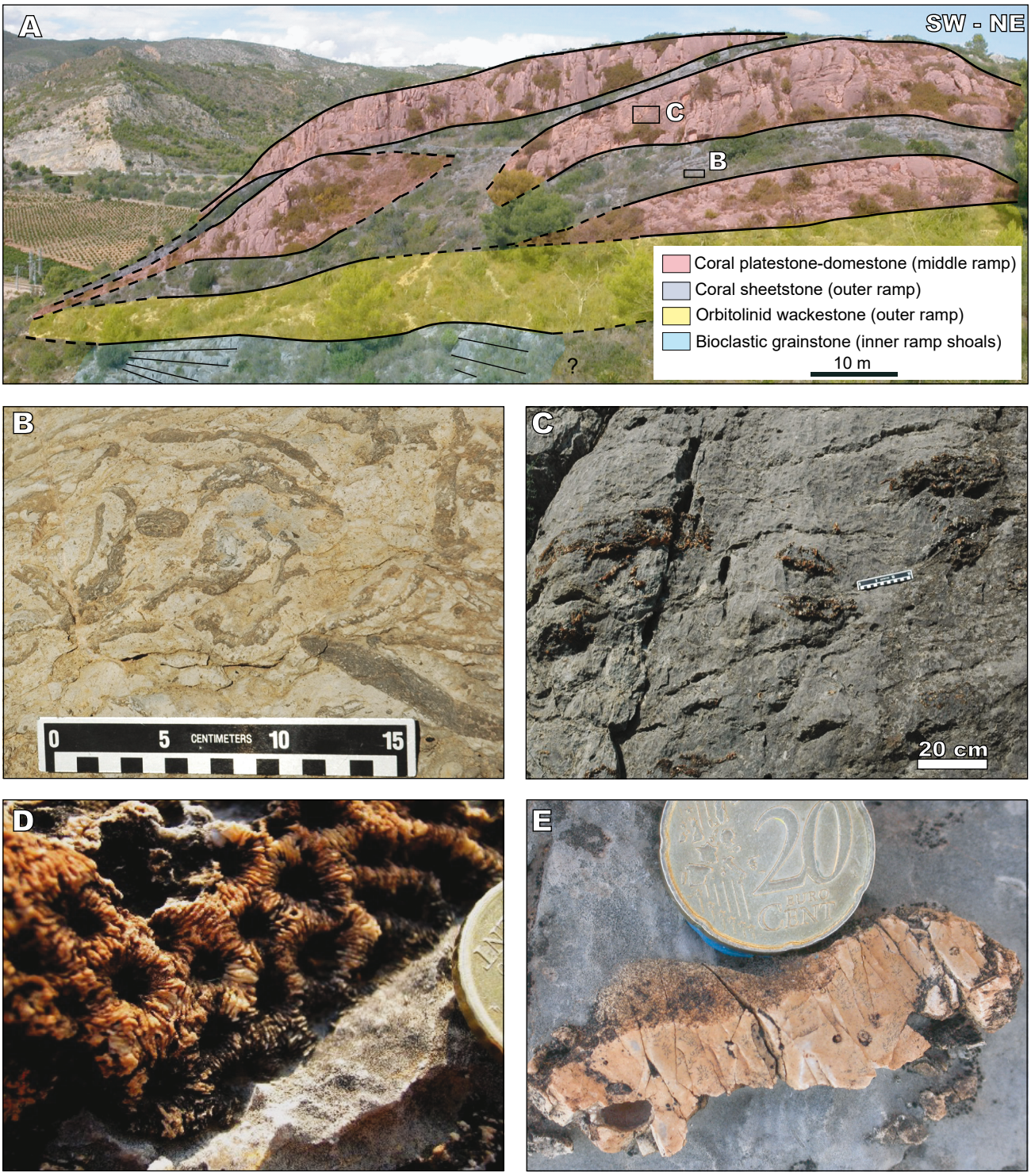

FIGURE 2. Outcrop photographs of the Aptian coral facies: A) View of La Venta section showing facies types and depositional environments. B) Coral sheetstones facies showing laminar corals (dark grey) and intervening particulate matrix (light brown). C) Coral platestone/domestone facies showing massive and tabular corals (dark grey), often partly silicified (orange veneer) and intervening matrix (light brown). D) Close-up view of a coral selectively replaced by silica. E) Close-up view of a silica nodule cement within the micritic matrix of the coral facies (grey).

Under CL, the detrital micrite shows dull red luminescence. Only locally, some areas are bright orange luminescence. The dense micrite and the peloidal matrix filling coral cavities exhibit homogeneous red luminescence, but the latter shows a greater heterogeneity, likely due to the presence of spar-filled fenestral cavities

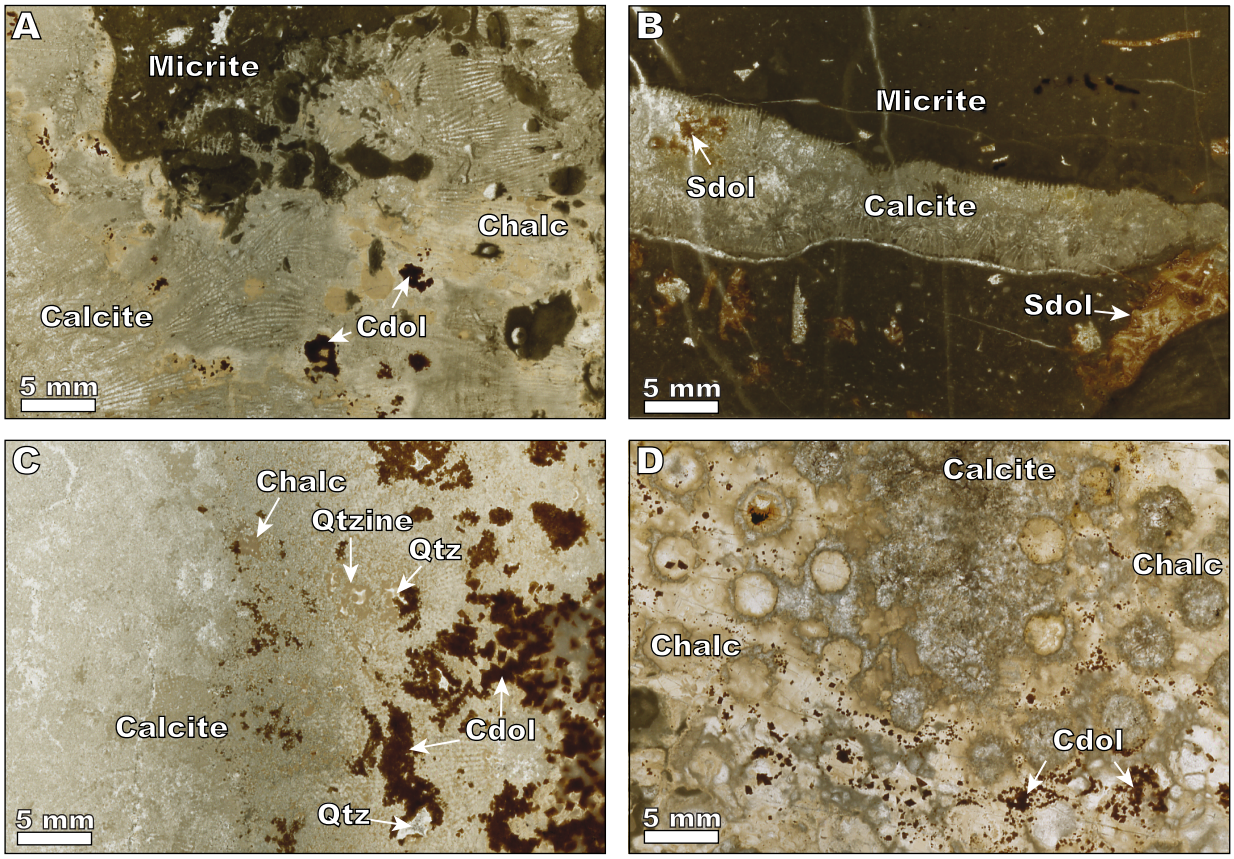

FIGURE 3. Thin section scan images of the coral facies. A) Coral (calcitic) partially replaced by chalcedony and calcitized dolomite. Note intervening particulate micrite. B) Coral (calcitic) partially replaced by saddle dolomite rhombohedra. Note intervening particulate micrite. C) Coral partially replaced by chalcedony and calcitized dolomite euhedral crystals. Note pore-filling quartzine and quartz cements and D) Recrystallized calcitic coral readily replaced by chalcedony and calcitized dolomite. Cdol= Calcitized dolomite; Chalc= Chalcedony; Sdol= Saddle dolomite; Qtzine= Quartzine; Qtz= Quartz.

(Fig. 4B). Micritic linings show red dull to non-luminescence (Fig. 4D).

Calcite 1 (Cc1)

Calcite Cc1 is characterized by well-developed euhedral crystals (often of approximately 150mm) that exhibit conspicuous and pervasive zoning under CL (Fig. 4). The most common zoning sequence consists of a non-luminescent core and a thin, bright orange luminescent outer zone (Fig. 4E). This zoning sequence can be repeated, and occasionally, the nucleus is followed by alternating bright-luminescent zones and dull bands. Cc1 occurs often as neomorphic calcite (*sensu* Folk, 1965) in the coral skeletons (Fig. 4C, D), but also as cement filling primary intra-skeletal pore spaces (Fig. 4A, B) or as microspar, product of the recrystallization of micrite. When neomorphic, it often exhibits fabric-selective mosaics (*sensu* Pingitore, 1976) that preserve the coral skeleton's structure. Cc1 is rarely observed filling secondary dissolution pores or fractures. In exceptional cases, Cc1 can develop spherulitic growth forms, ranging from hundreds of microns to few millimetres in diameter Under CL they display a small, bright orange nucleus coated by a wide, non-luminescent band mottled with dull red crystals, followed by a thin bright orange layer; this sequence is often repeated (Fig. 4F).

Calcite 2 (Cc2)

Calcite Cc2 is characterized by subhedral to anhedral crystals (ranging from 200mm to few millimetres in size), which are frequently twinned. Some crystals contain scattered (micritic) inclusions, giving them a "dirty" appearance. Under CL, Cc2 shows a dull orange luminescence, whereas the inclusions are bright orange (Fig. 4 A, B, G, H). Cc2 occurs exclusively as cement, filling primary intra-skeletal pores (Fig. 4A, B) as well as secondary dissolution pores and fractures (Fig. 4G, H) and clearly postdates calcite Cc1.

Calcite 3 (Cc3)

Calcite Cc3 is very scarce and consists of subhedral to anhedral crystals, up to 200mm in size. Cc3 crystals are

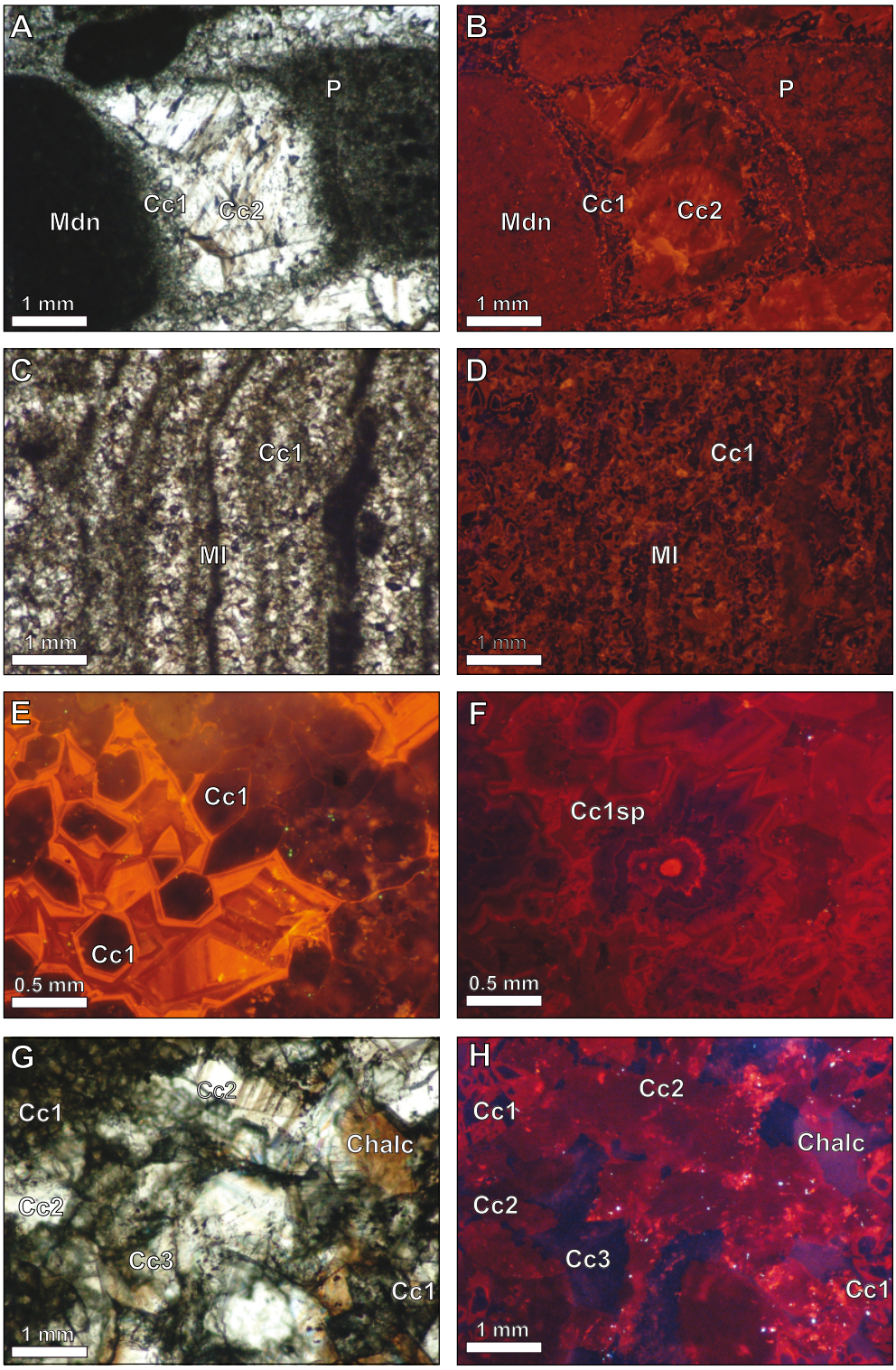

FIGURE 4. Photomicrographs of authigenic calcites. A-B) Neomorphic calcite Cc1 replacing coral skeleton and intra-skeletal cavities filled with calcite Cc2, micrite and peloidal matrix. Note the change in cathodoluminescence from zoned Cc1, non-luminescent core and a bright orange luminescent rim, to Cc2 dull orange. Dense micrite has homogeneous red luminescence and peloidal fabric shows more heterogeneity. Planed Polarized Light (PPL) and CathodoLuminescence (CL). C-D) Neomorphic calcite Cc1 replacing coral skeleton and micritic envelopes lining intra-skeletal pore spaces. Micritic linings have dull to non-luminescence (PPL and CL). E) Zoned euhedral Cc1 crystal with non-luminescent core and thin, bright orange luminescent outer zone (CL). F) Zoned spherulitic Cc1 crystal with small, bright orange nucleus coated by wide, non-luminescent band and, a thin bright orange layer. Note the repetition of the sequence (CL). G-H) Pore-filling calcite cements Cc1, Cc2 and Cc3 associated with chalcedony (PPL). Note the abrupt change in cathodoluminescence from zoned Cc1 to Cc2, dull orange, to Cc3 and Chalc, non-luminescent (PPL and CL). Cc1= Calcite 1; Cc1sp= spherulitic Calcite 1; Cc2= Calcite 2; Cc3= Calcite 3; Md= dense Micrite; Ml= Micrite Lining; P= Peloidal matrix; Chalc= Chalcedony.

very similar to those of Cc2 (twinned and with abundant impurities), but under CL, Cc3 is non-luminescent (Fig. 4G, H). Cc3 is only found filling secondary dissolution porosity and postdates calcite Cc2.

Calcite 4 (Cc4)

Calcite Cc4 has mm-scale crystals with variable morphologies, ranging from euhedral crystals, some with scalenohedron morphologies, to anhedral crystals (Fig. 5A-C). Under CL, Cc4 exhibits dull orange luminescence, but occasionally scattered bright orange spots appear within the crystals due to the presence of inclusions (iron oxides). Scalenohedrons also have a bright red nucleus (Fig. 5B). Cc4 scalenohedrons are found rimming large secondary pores, whereas Cc4 anhedral crystals occur in the centre of these pores. Calcite Cc4 clearly postdates diagenetic silica phases, such as quartzine and quartz (Fig. 5A-C).

Saddle dolomite (Sdol)

Saddle dolomite Sdol consists of brownish, subhedral to anhedral crystals of mm-scale, exhibiting a "dirty" appearance due to the presence of small carbonate inclusions. Locally, the dolomite develops rhombohedral forms with euhedral zoning. The faces of the crystals are curved and exhibit sweeping extinction, which is typical of saddle dolomite. Some crystals are twinned and/or show exfoliation planes. Sdol replaces corals and other bioclasts, either partially or totally (Figs. 3B; 5D). Under CL, Sdol shows a non-homogeneous dull orange luminescence, with one or more orange bright bands. No petrographic relationships have been observed between the saddle dolomite and the other diagenetic products.

Calcitized dolomite (Cdol)

Calcitized dolomite Cdol consists of isolated euhedral crystals, commonly exhibiting rhombohedral habits, ranging from 0.3 to 2mm in size, that replaces the host corals (Fig. 3A, C, D). They are dark brown in colour, due to the presence of abundant iron oxide inclusions (Fig. 5E). Although rhombohedrons are typical forms of dolomite, the elemental geochemistry indicates a calcite mineralogy (Table 1); thus, they correspond to calcitized dolomite. Under CL, Cdol crystals are usually zoned, with bright orange and thin dull brown bands (Fig. 5F). Rarely, non-zoned crystals are also observed. Cdol is commonly associated with different forms of silica (chalcedony, quartzine) and shows sharp contacts with them (Fig. 5E-G). Notably, small Cdol crystals are concentrated between the chalcedony and the calcitic coral skeleton, creating an amalgam of calcite, calcitized dolomite, and chalcedony, which imparts a "blurred" brownish appearance to the rock (Figs. 3C; 5H). Sometimes, dark brown calcitized dolomite with spherulitic habits has been observed at the rims of dissolution pores, replacing quartzine cements (Fig. 5C). This spherulitic calcitized dolomite shows no zonation under CL.

Silica

Silica occurs as ochre, to yellowish crystals of variable habits and forms (*i.e.* euhedral, spherulitic, pseudo-spherulitic, nodular) replacing the host corals with both, fabric-selectivity and/or cross-cutting fabrics (Fig. 3A, C, D). Only rarely, cm-scale silica nodules are observed in the matrix surrounding the corals (Fig. 2E). Replacive silica commonly consists of fibrous-shaped crystals of length-fast chalcedony (chalcedonite) and is frequently associated with Cdol crystals (Fig. 5C, E-H). In addition to

TABLE 1. Synthesis of the elemental composition of the calcites Cc1 to Cc4, the calcitized dolomite Cdol, and the saddle dolomite cement Sdol (mean ± standard deviation values are indicated for each element in ppm), and of calculated Mg/Ca, Sr/Ca, Ca/Fe and Mn/Ca fluid molar ratios of the parent fluid applying the distribution coefficient equation

	Na	Mg	Ca	Mn	Fe	Sr	Si	Mg/Ca (fluid)[a]	Mg/Ca (fluid)[b]	Sr/Ca (fluid)[c]	Ca/Fe (fluid)[d]	Mn/Ca (fluid)[e]
Cc1 (n= 67)	158±161	4,456±1,391	390,120±4,148	<d.l	630±794	895±240		0.162	1.57	0.017	5,362.33	?
Cc2 (n= 54)	<d.l.	4,301±1,255	390,876±3,858	287±99	1,116±819	1,006±645		0.156	1.51	0.019	3411	$6{\cdot}10^{-0.5}$
Cc3 (n= 9)	184±240	4,248±1,556	394,434±4,556	<d.l.	<d.l	1,271±465		0.152	1.48	0.024	?	?
Cc4 (n= 46)	<d.l.	4,414±979	387,201±3,209	<d.l	2,210±672	867±276		0.166	1.61	0.019	2,497.82	?
Cdol (n=46)	<d.l.	4,424±2,330	383,545±13,301	<d.l.	2,127±1,960	694±201	4,585±4,201					
Sdol (n=48)	401±1,006	76,432±56,506	290,679±78,954	189±72	1,074±1,188	725±255						

[a] k_{Mg}= 0.1163 at 90°C (Katz, 1973)
[b] k_{Mg}= 0.012 at 25°C (Mucci and Mors, 1983; Mucci, 1987; Burton and Walter, 1991)
[c] k_{Sr}= 0.06 at 25, 40, 98 and 200°C (Katz *et al.*, 1972; Stoessell *et al.*, 1987)
[d] k_{Fe}= 5 (Dromgoole and Walter, 1990)
[e] k_{Mn}= 8 (Dromgoole and Walter, 1990)
n= number of analyses
d.l.= detection limit

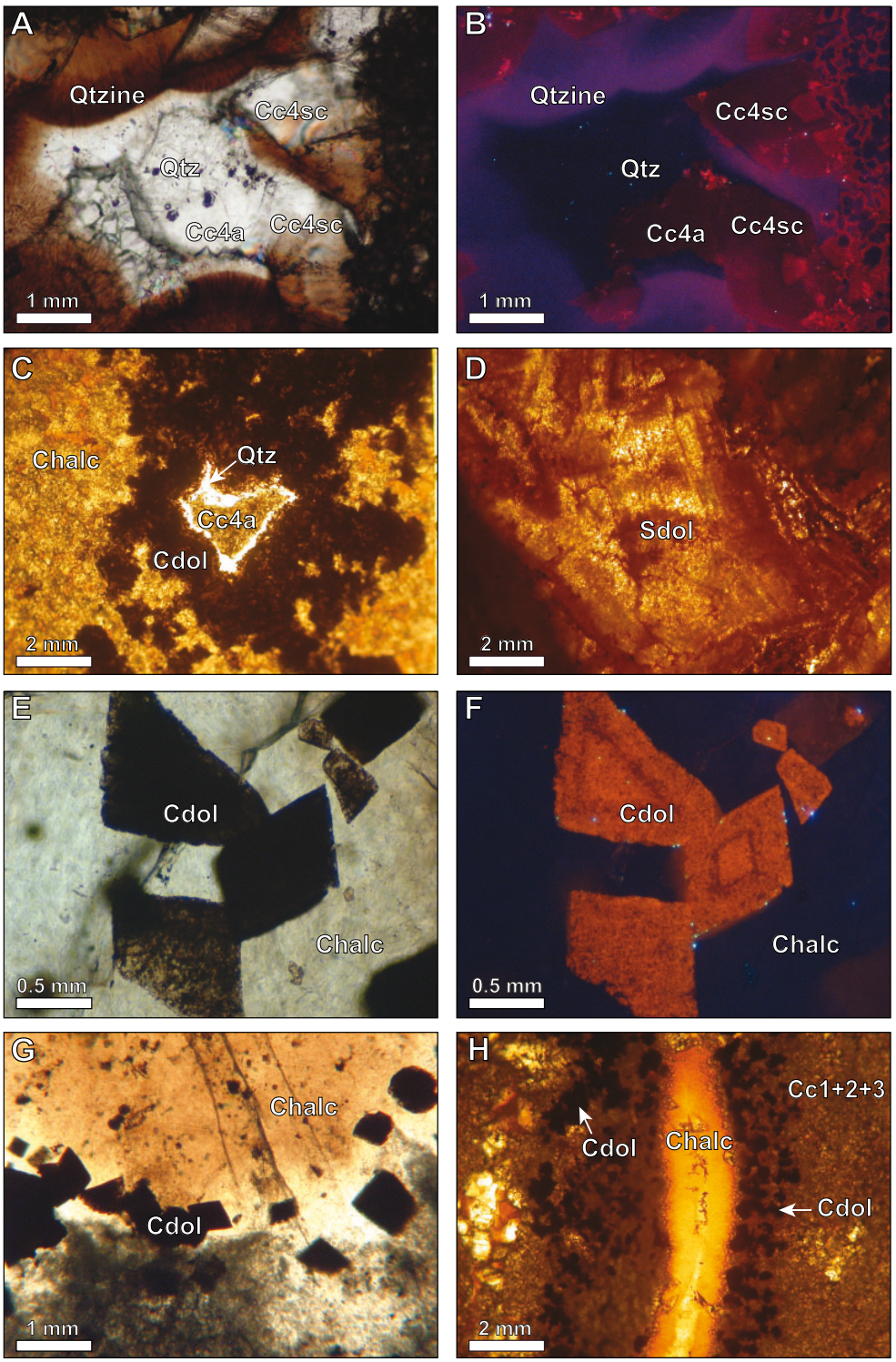

FIGURE 5. Photomicrographs of authigenic calcite, dolomite and silica. A-B) Secondary pore filled with spherulitic quartzine, calcite Cc4 (anhedral and scalenohedral forms) and quartz. Note the change in cathodoluminescence from Cc4, red dull luminescent crystals, to non-luminescent silica cements. Cc4 scalenohedra are zoned with bright luminescent core. Planed Polarized Light (PPL) and CathodoLuminescence (CL). C) Chalcedony and calcitized dolomite replacing coral skeletal structure. Secondary pore filled with Cc4 and quartz. Note the spherulitic-like morphology of calcitized dolomite likely replacing quartzine (PPL). D) Euhedral saddle dolomite crystal with characteristic curved faces and zonation (PPL). E-F) Calcitized dolomite rhombohedra associated with chalcedony. Note the bright orange luminescence and zonation of the rhombohedral crystals and the abrupt difference with the non-luminescent chalcedony (CL). G) Chalcedony and associated calcitized dolomite rhombohedra replacing coral skeletal structure (PPL). H) Calcitized dolomite euhedral crystals in the precipitation-dissolution chalcedony-calcite front. Note the amalgam of calcitized dolomite, chalcedony and calcite crystals in this alteration zone (PPL). Cc4a= anhedral calcite 4; Cc4sc= scalenohedral calcite 4; Qtzine= Quartzine; Qtz= Quartz; Cdol= Calcitized dolomite; Chalc= chalcedony; Sdol= Saddle dolomite; Cc1+2+3= calcite 1+2+3.

replacing length-fast chalcedony, other forms of silica, such as length-slow chalcedony (quartzine) and quartz, have been observed. The quartzine consists of orange to brown spherulites and pseudo-spherulites, approximately 1mm in size, that rim secondary pores (Fig. 5A, B). Locally, the quartzine spherulites can be replaced by calcitized dolomite (Fig. 5C) or by scalenohedrons of Cc4 (Fig. 5A, B). The quartz crystals form drusy mosaics that fills the centres of secondary pores (Fig. 5A, C). Under CL, all silica forms are either non-luminescent or exhibit blue luminescence (Fig. 5B, F).

Elemental geochemistry

The chemical composition of the different generations of calcite, calcitized dolomite, dolomite, and silica was analysed using an electron microprobe. The concentrations of Ca, Mg, Sr, Mn, Fe and Na were measured in all identified carbonates. Additionally, Si content was measured in the calcitized dolomites due to their close association with the silica forms. The results are presented in Table 1.

In all carbonates the Na content is below or close to the detection limit (varying from 158 to 184ppm), except for the saddle dolomite Sdol which averages 400ppm. Similarly, Mn is undetectable or just at the detection limit (189ppm), only reaching 287ppm on average in Cc2. All calcites have similar Mg concentrations ranging between 4,200 and 4,400ppm, which are the expected values for LMC; in the Sdol the Mg content reaches up to 76,400ppm. What varies most in all identified carbonates is the content of Fe and Sr. The Fe content is low in Cc1 (630ppm on average) and undetectable in Cc3 but increases significantly in Cc2 (1,116ppm on average) and even more in Cc4 (2,210ppm on average). The Fe values in the calcitized dolomite Cdol are similar to that of Cc4 (2,127ppm on average) and in Sdol to that of Cc2 (1,074ppm on average). The Sr values are similar in Cc1 and Cc4 with average concentrations of 895 and 867ppm, respectively. The content increases to 1,006ppm on average in Cc2, and to 1271ppm on average in Cc3, the latter being the highest among all carbonates. Cdol and Sdol show clearly lower Sr concentrations (694 and 725ppm on average, respectively). Si is only present in Cdol, likely due to its association with diagenetic chalcedony and quartz.

Moreover, the element molar ratios (Mg/Ca, Ca/Fe, Sr/Ca and Mn/Ca) of the calcites (Cc1, Cc2, Cc3, Cc4) were calculated (Table 1). Assuming that precipitation occurs in equilibrium, the elemental composition of the fluid from which calcite precipitates can be estimated by using the chemical composition of the carbonate (*e.g.* Banner and Hanson, 1990; Meyers and Lohmann, 1985) and the distribution coefficient equation of McIntire (1963):

$$D = (Tr/Cr)_S / (Tr/Cr)_L \quad (1)$$

where D= partition coefficient; (Tr/Cr)= ratio of the concentration of the trace element to that of the carrier element; S= solid phase; L= liquid phase.

The data are compared with molar ratios typical of marine fluids (Mg/Ca= 5.3, Ca/Fe>10,000, Sr/Ca= 0.86 x 10^{-2}, Mn/Ca= 3x10^{-7}; Travé *et al.*, 1997, 2000 and references therein and Mg/Ca ranging from 1 to 6.5; Huck and Heimhofer, 2021) , of meteoric fluids (Mg/Ca ranging from 0.05 to 1.4, Ca/Fe>1,000, Sr/Ca= 0.32 x 10^{-2} and Mn/Ca= 0.25 x 10^{-3}; Travé *et al.*, 1997, 2000 and references therein) and formation waters (Mg/Ca ranging from 0.05 to 1.4, Ca/Fe> 100, Sr/Ca ranging from 0.01 to 0.15 and Mn/Ca~7x10^{-5}; Travé *et al.*, 1997, 2000 and references therein).

Oxygen and carbon isotopic geochemistry

Isotope analyses were conducted on the various types of carbonates observed. Calcite Cc3 could not be analysed due to the sub-millimetric crystal size, which made it difficult to identify with the naked eye and therefore separate with manual sampling. Similarly, silicates were excluded from analysis, as it was not possible to separate and obtain a sufficient sample quantity of each form.

A total of 36 samples between host rocks (micrite) and carbonate diagenetic products were analysed for their stable isotopic composition. The data are shown in Table 2 and Figure 6. The micrite host-rock shows $\delta^{18}O$ values between -4.7 and -3.4‰VPDB and $\delta^{13}C$ values ranging from -0.3 to +2.2‰VPDB. Due to challenges in separating Cc1 and Cc2, some samples may exhibit a slight cross-contamination. These early calcite types show $\delta^{18}O$ values ranging from -5.9 to -3.2‰ and $\delta^{13}C$ values varying from +0.2 to +2.9‰. Calcitized dolomites have $\delta^{18}O$ values from -7.1 to -5.3‰, and $\delta^{13}C$ values from -4.1 to -2.1‰. Cc4 has $\delta^{18}O$ values ranging from -8.5 to -7.9‰ and $\delta^{13}C$ values from +2.6 to +2.7‰. Finally, saddle dolomite samples exhibit $\delta^{18}O$ values from -7.9 to -6.5‰ and $\delta^{13}C$ values ranging from +3.1 to +4.1‰.

The isotopic composition and temperature of the fluid from which calcite cements precipitated have been inferred using Craig's (1965) equation:

$$T(^{o}C) = 16.9 - 4.2 * (\delta^{18}O_{calcite(VPDB)} - \delta^{18}O_{water}) + 0.13 * (\delta^{18}O_{calcite\ (VPDB)} - \delta^{18}O_{water})^2 \quad (2)$$

To determine the composition and temperature of the fluids from which dolomite cements precipitated, we used the equation proposed by Friedman and O'Neil (1977):

$$T(^{o}K) = (3.2 * 10^6 / (\delta^{18}O_{dolomite\ (SMOW)} - \delta^{18}O_{water}) + 1.5)^{0.5} \quad (3)$$

TABLE 2. Measured isotopic values of the host-rock micrite, the calcites Cc1, Cc2, Cc4, the calcitized dolomite (Cdol rep and Cdol pore) and the saddle dolomite cement Sdol

	$\delta^{18}O$‰VPDB	$\delta^{13}C$‰VPDB		$\delta^{18}O$‰VPDB	$\delta^{13}C$‰VPDB
Micrite	-3.54	2.22	Cdol rep	-5.72	-3.01
Micrite	-3.40	1.57	Cdol rep	-6.43	-2.86
Micrite	-4.30	-0.32	Cdol rep	-6.09	-3.03
Micrite	-4.67	1.01	Cdol rep	-6.89	-3.89
Micrite	-3.64	1.14	Cdol rep	-5.78	-3.03
Cc1	-4.51	2.79	Cdol rep	-6.65	-4.15
Cc1	-5.05	1.29	Cdol rep	-7.15	-3.35
Cc1 (Cc2)	-4.54	1.07	Cdol rep	-6.64	-2.93
Cc1 (Cc2)	-5.45	2.94	Cdol pore	-5.33	-2.25
Cc2	-4.74	2.80	Cdol pore	-5.35	-2.12
Cc2	-5.06	2.75	Sdol	-7.55	3.17
Cc2 (Cc1)	-5.32	2.83	Sdol	-6.50	3.09
Cc2 (Cc1)	-5.93	2.73	Sdol	-7.77	4.07
Cc2 (Cc1)	-4.67	2.72	Sdol	-7.95	4.01
Cc2 (Cc1)	-3.84	0.71	Sdol	-7.27	4.00
Cc2 (Cc1)	-3.26	0.59	Sdol	-7.03	4.08
Cc4	-8.52	2.69	Sdol	-7.46	4.09
Cc4	-7.88	2.78	Sdol	-7.38	3.97

Ccx(Ccy)= sample of x possibly contaminated with y

Equations (1) and (2) were applied to the measured $\delta^{18}O$ values of each calcite and dolomite type, considering different $\delta^{18}O_{water}$ values based on petrographic features and elemental geochemistry data. The following $\delta^{18}O$ reference values were used: -3‰ SMOW for Cretaceous marine waters (Veizer *et al.*, 1980, 1999), -6‰ SMOW for meteoric waters, and +2‰ SMOW for formation brines. The calculated temperatures are shown in Table 3.

DISCUSSION

The diagenetic sequence observed in the studied coral-bearing facies can be divided into three main stages: i) precipitation of Cc1, Cc2, Cc3, silicification and dolomitization during early diagenesis, at shallow-burial, from mixing meteoric and marine waters, ii) precipitation of saddle dolomite and Cc4 calcite cement during intermediate burial diagenesis, from hot waters and iii) dedolomitization during late diagenesis (uplift) from meteoric waters (Fig. 7).

Early Calcites

The micrite host-rock with $\delta^{18}O$ values ranging from -4.7 to -3.4‰ and $\delta^{13}C$ values between -0.3 to +2.2‰ are consistent with the global isotope values typically seen in Cretaceous marine carbonate sediments (Huck and Heimhofer, 2021; Veizer and Hoef, 1976; Veizer *et al.*, 1980, 1999).

Cc1 and Cc2 show similar isotopic values with $\delta^{18}O$ ranging from-5.9 to -3.2‰ and $\delta^{13}C$ from +0.6 to +2.9‰ that agree with those of the marine host-rock suggesting high fluid-rock interaction. Moreover, the slight depletion of $\delta^{18}O$ values would indicate meteoric water influence in syn-sedimentary marine conditions at very shallow burial depths during early diagenesis. The Mg/Ca molar ratio values of Cc1 and Cc2 (around 1.5) indicate precipitation from shallow marine waters (Huck and Heimhofer, 2021) and/or meteoric waters (from 0.05 to 1.4; Travé *et al.*, 1997, 2000 and references therein). In Cc1, low Fe and undetectable Mn contents and high Na content suggests more marine conditions. In Cc2 the higher Fe and Mn content and the lower Na values suggest more meteoric conditions. Thus, these early calcites Cc1 and Cc2 would have precipitated from mixing meteoric and shallow-marine waters, so that their fluid-precipitation temperatures would range between 6 and 31ºC (Table 3). The possibility of precipitation from formation waters is ruled out due to the petrographic characteristics and geochemical data of

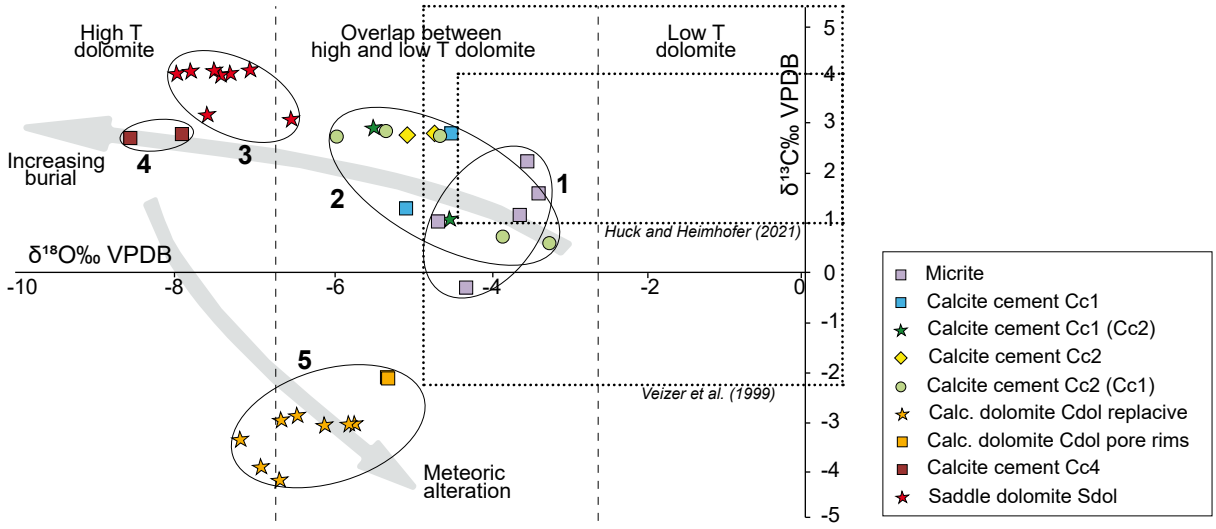

FIGURE 6. Plot of $\delta^{13}C$ vs. $\delta^{18}O$ for the micrite and diagenetic phases of the Benassal Formation carbonates. Values of Cretaceous marine carbonates (dotted line polygons), according to Veizer *et al.* (1999) for open marine signals and to Huck and Heimhofer (2021) for shallow marine signals. The isotopic composition of the saddle dolomite is compared with the precipitation temperatures of dolomites proposed by Allan and Wiggins (1993), represented by vertical dashed lines. Areas traced by full lines correspond to diagenetic processes and their relative timing: 1) Host-rock micrite formation, 2) Early calcite (Cc1 and Cc2) cementation, 3) Saddle dolomite formation, 4) Burial calcite (Cc4) cementation and 5) Meteoric calcitization of previously formed dolomite.

these early calcites. Neomorphic Cc1 with fabric-selective mosaics preserving the coral skeletal structure imply an early transformation of the initial aragonite into calcite. The neomorphic process in the corals might have been very rapid and syn-depositional, as it has been reported from modern corals, molluscs and bryozoans (*e.g.* James *et al.*, 2005; Maliva, 1998). Moreover, the zoned CL pattern of Cc1 COULD be related to changes in the redox conditions in nearshore environments (Hood and Wallace, 2015).

The Mg/Ca molar ratio values of Cc3, similar to those of Cc1 and Cc2, can be interpreted either as precipitated from shallow marine waters and/or meteoric fluids. However, very low or undetectable Fe and Mn values, Na values slightly higher than Cc2 and the highest Sr content, suggest a return to stronger marine conditions.

In sum, it is reasonable to conclude that the diagenetic calcite forms Cc1, Cc2, and Cc3 precipitated from mixed waters rather than exclusively marine or meteoric sources, where Cc1 and Cc3 likely formed in meteoric waters with a stronger shallow-marine influence and Cc2 under higher meteoric influence.

Early calcites: Relationships with relative sea-level fluctuations

The variations in elemental composition can potentially be explained by relative sea-level fluctuations. Initially, micritization, coral neomorphism, and the precipitation of cement Cc1 within primary pores occurred under marine conditions with meteoric influence. Subsequently, the primary pores were filled with Cc2, whose composition indicates precipitation from a fluid with a higher meteoric influence, likely during a relative sea-level drop, which led to the formation of the first dissolution pores. The precipitation of Cc3 in the secondary pores indicates a return to more marine conditions, suggesting a relative rise of sea level.

Moreover, the varying amounts and textures observed in calcites Cc1, Cc2 and Cc3 may also relate to changes in the phreatic environment, transitioning from stagnant to more active zones. Even in fully saturated environments, variations in water movement rates through the sediment can significantly impact the cementation process. In stagnant phreatic zones, water movement is slow, resulting in minimal cementation (as seen in Cc1 and Cc3), and little effect on total skeletal porosity. Such zones are typically found in lagoons, deeper parts of sloping ramps, or distal talus areas (Longman, 1980; Swei and Tucker, 2012). In contrast, active zones, where water flows readily into the sediment, results in increased rates of cementation (as seen in Cc2). These active zones are often associated with shelf margins, reefs, or sediments of the upper shoreface (Longman, 1980). The transition from stagnant to active zones are directly related to changes in the water column related to relative sea-level fluctuations. The precipitation of fabric-selective calcite, such as Cc1, would occur in tranquil marine environments with minimal water circulation. A drop in relative sea level would likely enhance water circulation, potentially due to the influx of meteoric waters (Longman, 1980; Swei and Tucker, 2012).

TABLE 3. Synthesis of the isotopic composition and precipitation temperature of the fluids from which the calcites Cc1-Cc2, Cc4, the calcitized dolomite Cdol, and the saddle dolomite Sdol could have precipitated. Calculations are done with the maximum, minimum and mean $\delta^{18}O$ values and considering standard mean values of meteoric waters (-6‰ SMOW), Cretaceous marine limestones (-3‰ SMOW) and formation waters/brines (+2‰ SMOW). Samples of Cc1 and Cc2 may be slightly contaminated with each other

		$\delta^{18}O$‰VPDB rock	$\delta^{18}O$‰VPDB water	T(ºC)		$\delta^{18}O$‰VPDB rock	$\delta^{18}O$‰VPDB water	Tº(C)
Max.	Cc1-Cc2	-6	-3	31	Cdol	-7.1	-3	65
Min.	Cc1-Cc2	-3.2	-3	18	Cdol	-5.3	-3	54
Mean	Cc1-Cc2	-4.6	-3	24	Cdol	-6.2	-3	59
Max.	Cc1-Cc2	-6	-6	17	Cdol	-7.1	-6	48
Min.	Cc1-Cc2	-3.2	-6	6	Cdol	-5.3	-6	39
Mean	Cc1-Cc2	-4.6	-6	11	Cdol	-6.2	-6	43
Max.	Cc4	-8.5	-3	44	Cdol	-7.1	+2	100
Min.	Cc4	-7.9	-3	41	Cdol	-5.3	+2	86
Mean	Cc4	-8.2	-3	42	Cdol	-6.2	+2	93
Max.	Cc4	-8.5	-6	28	Sdol	-8	-3	71
Min.	Cc4	-7.9	-6	25	Sdol	-6.5	-3	61
Mean	Cc4	-8.2	-6	27	Sdol	-7.25	-3	66
Max.	Cc4	-8.5	+2	75	Sdol	-8	-6	53
Min.	Cc4	-7.9	+2	71	Sdol	-6.5	-6	45
Mean	Cc4	-8.2	+2	73	Sdol	-7.25	-6	49
Max.					Sdol	-8	+2	107
Min.					Sdol	-6.5	+2	95
Mean					Sdol	-7.25	+2	101

Ccx-Ccy= samples may be slightly contaminated with each other

Dolomitization and silicification: Are they linked processes?

Silicification clearly post-dates Cc1, Cc2, and Cc3 (Fig. 5G, H), and manifests primarily as chert nodules that selectively replace coral skeletons, or occasionally bivalve shells, occluding skeletal porosity. Jacka (1974) reported selective replacement of fossils by chalcedony, attributing this to the micro-environment created by the decomposition of organic matter, which favoured silica replacement. The absence of silica replacement in the micrite matrix or intraclasts led Jacka to argue that silicification occurred, prior to matrix deposition, during very early diagenesis.

In areas of silica-replacement, dolomite crystals often appear "floating", particularly along the silica growth front (Fig. 5H). The interplay between silicification and dolomitization has been widely documented (Al-Dabbagh and El-Sorogy, 2016; Alonso-Zarza *et al.*, 2002; Bustillo and La Iglesia, 1978; Donnelly and Merrill, 1977; Erragragui *et al.*, 2023; Jacka, 1974; Knauth, 1979, 1994; Misik, 1968; Walker, 1960, 1962). Observed petrographic relationships in this study suggest a complex chronology for these processes (Fig. 7). In some instances, dolomite replaces chalcedony, adopting chalcedony's spherulitic morphology (Fig. 5C). Conversely, dolomite crystals occur within the silica growth front, preceding silica (Fig. 5H). In these cases, a mix of calcite, chalcedony, and dolomite (now calcitized) is present at the contact between the host rock and silica nodules. This supports Jacka's (1974) hypothesis of contemporaneous silica and dolomite formation, which suggested that silica replacement occurred before the original HMC skeletal particles stabilized to LMC, releasing magnesium that would facilitate dolomitization. The original coral skeleton mineralogy was likely aragonitic (Early Cretaceous) and elemental geochemistry suggests that the transformation from aragonite to LMC and the dissolution of aragonite occurred synchronously to the precipitation of the early calcites.

According to Knauth (1979, 1994), the silicification of marine carbonates forms through the leaching of biogenic silica by meteoric waters, and its coexistence with dolomite indicates that the diagenetic environment was shallow, with

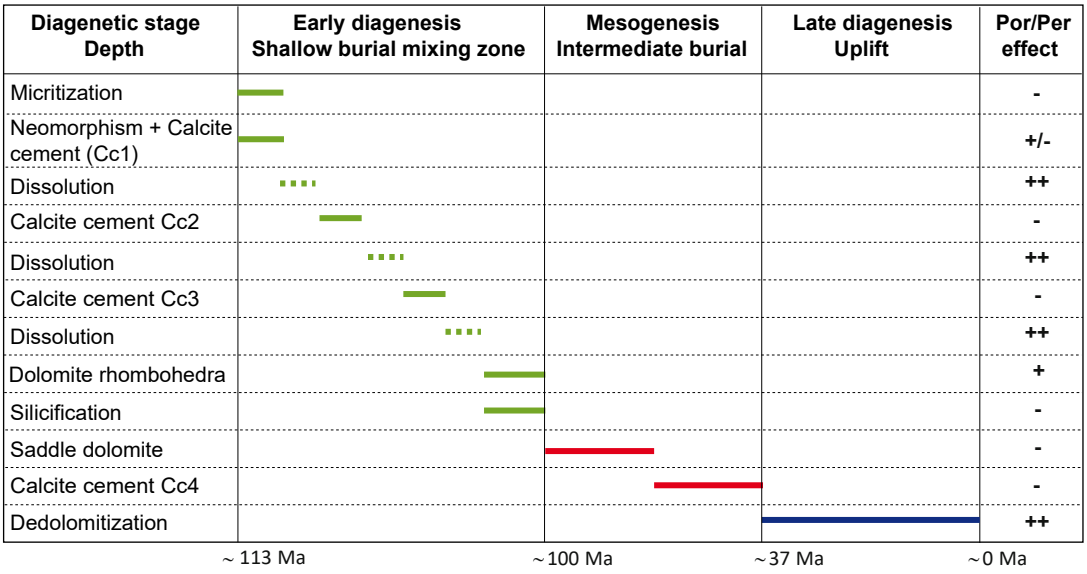

FIGURE 7. Paragenetic sequence showing the relative timing of most important diagenetic events. Green= mixing of meteoric and marine waters, blue= meteoric water, red= formation water, por-per effect= porosity-permeability effective. Chronology is based on Martín-Martín *et al.* (2015).

a mixture of marine and meteoric waters. Under these conditions, calcite and aragonite dissolve, while silica and dolomite precipitate. On the other hand, Kidder and Erwin (2001) demonstrate that the Cretaceous was a period marked by an increase in biogenic silica in the oceans, a factor that would have favoured the silicification of marine limestones formed during the Aptian, as is the case of the Benassal Formation.

Other authors have suggested that chertification is a late diagenetic process occurring post-burial under meteoric conditions (Maliva and Siever, 1989; Whittle and Alsharhan, 1994). However, in our study, the coexistence of silica with dolomite points to a shallow diagenetic setting.

Si and Mg sources

The silica source was likely biogenic, derived from in-situ sponge spicule dissolution, which are abundant in the host limestone. Progressive burial increases temperature and silica solubility, promoting sponge spicules dissolution and chert precipitation.

The dolomites likely precipitated from a mix of marine and meteoric fluids. The Mg for dolomite formation may have been released from the neomorphic transformation of the original aragonite coral skeletons to Low Magnesium Calcite (LMC) during very early diagenesis, when carbonate was still partially lithified (Jacka, 1974), dissolution of biogenic components and early calcites during silicification. Alternatively, Donelly and Merrill (1977) proposed that Mg could originate from biogenic opal to quartz transformations.

Late carbonate cements: saddle dolomite, Cc4, and dolomite calcitization

The saddle dolomite has more negative $\delta^{18}O$ values (-7.9 to -6.5‰; Table 2; Fig. 6) than the early calcites that are consistent with higher temperature fluids, likely at intermediate burial conditions, as evidenced by its petrographic features (Machel, 1987; Radke and Mathis, 1980; Spölt and Pitman, 1998). High temperatures, approximately 95 to107ºC, are obtained from formation brines ($\delta^{18}O$=+2‰ SMOW) (Table 3); these temperatures are consistent with saddle dolomite formation involving minima of 80ºC (Davies and Smith, 2006) or ranges of 50 to 150ºC (Choquette and James, 1987).

A later stage of calcite precipitation (Cc4) occurred, possibly under similar burial and temperature conditions than the saddle dolomite, as indicated by the depleted values of $\delta^{18}O$, varying from -8.5 to -7.9‰. The molar ratios of the mineralizing fluids of Cc4 agree with formation brines. Assuming a $\delta^{18}O$ value of approximately +2‰ SMOW for these brines, precipitation may have occurred at around 70ºC (Table 3). Although the chronology between saddle dolomite and Cc4 could not be established in this work, regional studies show that saddle dolomite precedes late-stage calcites (Humphrey *et al.*, 2022; Martín-Martín *et al.*, 2015).

Finally, the negative $\delta^{18}O$ values (-7.1 to -5.3‰) and $\delta^{13}C$ values (-4.1 to -2.1‰) of the calcitized dolomites suggests that calcitization occurred from meteoric waters, likely during late diagenesis related to uplift, as already suggested by Martín-Martín *et al.* (2015) and Centrella

et al. (2023) in nearby areas of Benicàssim. Calcitization occurred at temperatures ranging from 21 to 48ºC (Table 3). The negative $\delta^{13}C$ values in all calcitized dolomites may indicate organic matter involvement in oxidation or bacterial sulphate reduction processes.

CONCLUSIONS

This work shows that early diagenetic products of coral facies can be linked to paleoenvironmental controls. Specifically, the integration of petrography, elemental geochemistry and stable (C and O) isotopes allow us to reconstruct sea-level fluctuations during the Aptian. The same approach can be applied in other sites or geological intervals with shallow-water corals.

Cc1 and Cc3 are likely formed in a mixing zone with significant marine influence (relative sea-level rise), whereas Cc2 shows a stronger meteoric water influence (relative sea-level drop). Under similar conditions, silica and isolated rhombohedral dolomite precipitated.

This study highlights the interplay between dolomitization and selective silicification in corals, commonly observed in biogenic components through the geological record. Both processes are coetaneous and occur in very shallow environments from a mixture of marine and meteoric waters. The silica phases likely originated from the biogenic dissolution of sponge spicules, while the Mg required for dolomite formation may have been released from the neomorphic transformation of the original aragonite coral skeletons to LMC, and from the dissolution of biogenic components and early calcites.

Late carbonate cements also have an impact on shallow-water coral facies. Saddle dolomite and Cc4 formed during intermediate burial from high-temperature brines. The calcitization of dolomite occurred during late diagenesis (uplift) under the influence of meteoric waters.

The results of this study provide valuable insights into the complex diagenetic history of fossil scleractinian corals, from very early- to late diagenesis, as well as the interrelationships between authigenic calcite, dolomite, and silica, and the nvironmental conditions under which they formed.

ACKNOWLEDGMENTS

Authors are grateful to Rute Coimbra and María Najarro for their constructive comments, and to editor Telm Bover-Arnal for his valuable advice. This work is part of the project PID2021-12246NB-C22 funded by MICIU/AEI/10.13039/501100011033 and by FEDER, UE and the Catalan Council to the Grup Consolidat de Recerca Reconegut Geologia Sedimentària (2021 SGR-Cat 00349).

REFERENCES

Al-Dabbagh, M.E., El-Sorogy, A.S., 2016. Diagenetic alterations of the upper Jurassic scleractinian corals, Hanifa Formation, Jabal Al-Abakkayn, central Saudi Arabia. Journal of the Geological Society of India, 87(3), 337-344.

Allan, J.R., Wiggins, W.D., 1993. Dolomite reservoirs-geochemical techniques for evaluating origin and distribution. American Association of Petroleum Geologists (AAPG), Continuing Education Course, Note Series, 36, 129pp.

Allison, N., Finch, A.A., Webster, J. M., Clague, D.A., 2007. Palaeoenvironmental records from fossil corals: the effects of submarine diagenesis on temperature and climate estimates. Geologica et Cosmochimica Acta, 71(19), 4693-4703.

Alonso-Zarza, A.M., Sánchez-Moya, Y., Bustillo, M.A., Sopeña, A., Delgado, A., 2002, Silicification and dolomitization of anhydrite nodules in argillaceous terrestrial deposits: an example of meteoric-dominated diagenesis from the Triassic of central Spain. Sedimentology, 49, 303-317.

Andrade, C.N., Chafetz, H.S., Lapen, T.J., 2020. Paragenesis of silicified mid-Paleozoic and mid-Cenozoic corals based on petrography and silicon isotopic analyses. Chemical Geology, 538, 119483.

Badali, M., 2003. Paleoenvironments, diagenesis, and sequence stratigraphy of the mid-cretaceous section (Albian/Cenomanian) in the main pass field area, Northeastern Gulf of Mexico. Carbonates and Evaporites, 18, 29-40.

Banner, J.L., Hanson, G.N., 1990. Calculations of simultaneous isotopic and trace element variations during water-rock interaction with applications to carbonate diagenesis. Geochimica et Cosmochimica Acta, 54, 3123-3137.

Bathurst, R.G., 1975. Carbonate sediments and their diagenesis. Amsterdam, Elsevier, 660pp.

Bover-Arnal, T., Moreno-Bedmar, J.A., Frijia, G., Pascual-Cebrian, E., Salas, R., 2016. Chronostratigraphy of the Barremian-Early Albian of the Maestrat Basin (E Iberian Peninsula): integrating strontium-isotope stratigraphy and ammonoid biostratigraphy. Newsletters on Stratigraphy, 49, 41-68.

Burton, E.A., Walter, L.M., 1991. The effects of P_{CO2} and temperature on magnesium incorporation in calcite in seawater and $MgCl_2$-$CaCl_2$ solutions. Geochimica et Cosmochimica Acta, 55, 777-785.

Bustillo, M.A., La Iglesia, A., 1978. Procesos de formación y diagénesis en las rocas silíceas de Sangunto. Estudios Geológicos, 34, 167-174.

Centrella, S., Beaudoin, N.E., Trebucq, C., Hoareau, G., Gomez-Rivas, E., Martín-Martín, J.D., Callot, J.P., 2023. Textural and chemical evolution during dedolomitization: A case study of the Benassal Formation, Maestrat Basin, Spain. Marine and Petroleum Geology, 153, 106290.

Choquette, P.W., James, N.P., 1987. Diagenesis #12. Diagenesis in limestone-3. The deep burial environment. Geoscience Canada, 14, 3-34.

Craig, H., 1965. Measurement of oxygen isotope paleotemperatures. In: Tongiorgi, E. (ed.). Stable Isotopes in Oceanographic Studies and Paleotemperatures. Pisa, Consiglio Nazionale delle Ricerche, Laboratorio di Geologia Nucleare, 161-182.

Craig, H., Gordon, I., 1965. Deuterium and oxygen-18 variations in the ocean and the marine atmosphere. In: Tongiogi, E. (ed.). Stable Isotopes in Oceanographic Studies and Paleotemperatures. Pisa, Consiglio Nazionale delle Ricerche, Laboratorio di Geologia Nucleare, 9-130.

Davies, G.R., Smith Jr., L.B., 2006. Structurally controlled hydrothermal dolomite reservoir facies: An overview. American Association of Petroleum Geologists (AAPG) Bulletin, 90, 1641-1690.

Donnelly, W., Merrill, L., 1977. The scavenging of magnesium and other chemical species by biogenic opal in deep–sea sediments. Chemical Geology, 19, 167-187.

Dromgoole, E.L., Walter, L.M., 1990. Iron and manganese incorporation into calcite: Effects of growth kinetics, temperature and solution chemistry. Chemical Geology, 81, 311-336.

El-Saiy, A.K., Jordan, B.R., 2007. Diagenetic aspects of tertiary carbonates west of the Northern Oman Mountains, United Arab Emirates. Journal of Asian Earth Sciences, 31(1), 35-43.

Enmar, R., Stein, M., Bar-Matthews, M., Sass, E., Katz, A., Lazar, B., 2000. Diagenesis in live corals from the gulf of Aqaba. I. The effect on paleo-oceanography tracers. Geochimica and Cosmochimica Acta, 64(18), 3123-3132.

Erragragui, M., Masrour, A., Benbaqqal, H., Jilali, A., 2023. Diagenetic evolution and carbonate reservoir quality of the Domerian-Bajocian South-Rifain Ridges, Morocco. Journal of African Earth Sciences, 200, 104860.

Friedman, G.M., Amiel, A.J., Scneidermann, N., 1974. Submarine cementation in reefs: example from the Red Sea. Journal of Sedimentary Petrology, 44, 816-825.

Friedman, I., O'Neil, J.R., 1977. Compilation of stable isotope fractionation factors of geochemical interest. US Geological Survey, Professional Paper, 440-kk.

Gomez-Rivas, E., Corbella, M., Martín-Martín, J.D., Stafford, S.L., Teixell, A., Bons, P.D., Griera, A., Cardellach, E., 2014. Reactivity of dolomitizing fluids and Mg source evaluation of fault-controlled dolomitization at the Benicàssim outcrop analogue (Maestrat Basin, E Spain). Marine and Petroleum Geology, 55, 26-42.

Gomez-Rivas, E., Warber, K., Kulzer, F., Bons, P.D., Koehn, D., Martín-Martín, J.D., 2012. Structural evolution of the Benicàssim area (Maestrat basin, NE Spain): insights from fracture and vein analysis. Geogaceta, 51, 79-82.

Hood, V.S.A., Wallace, M.W., 2015. Extreme Ocean Anoxia during the Late Cryogenian Recorded in Reefal Carbonates of Southern Australia. Precambrian Research, 261, 96-111.

Huck, S., Heimhofer, U., 2021. Early Cretaceous sea surface temperature evolution in subtropical shallow seas. Scientific Reports, 11(1), 19765.

Humphrey, E., Gomez-Rivas, E., Martín-Martín, J.D., Neilson, J., Salas, R., Guimerà, J., 2022. Depositional and structural controls on a fault-related dolostone formation (Maestrat Basin, E Spain). Basin Research, 34, 961-990.

Insalaco, E., 1998. The descriptive nomenclature and classification of growth fabrics in fossil scleractinian reefs. Sedimentary Geology, 118, 159-186.

Jacka, A.D., 1974. Replacement of fossils by length–slow chalcedony and associates dolomitization. Journal of Sedimentary Petrology, 44, 421-427.

James, N.P., Ginsburg, R.N., Marzalek, D.S., Choquette, P.W., 1976. Facies and fabric specificity of early subsea cements in shallow Belize (British Honduras) reefs. Journal of Sedimentary Petrology, 46, 523-544.

James, N.P., Bone, Y., Kyser, T.K., 2005. Where has all the aragonite gone? Mineralogy of Holocene neritic cool-water carbonates, southern Australia. Journal of Sedimentary Research, 75, 454-463.

Katz, A., 1973. The interaction of magnesium with calcite during crystal growth at 25-90°C and one atmosphere. Geochimica et Cosmochimica Acta, 37, 1563-1586.

Katz, A., Sass, E., Starinsky, A., Holland, H.D., 1972. Strontium behavior in the aragonite-calcite transformation: An experimental study at 40-98°C. Geochimica et Cosmochimica Acta, 36, 481-496.

Kidder, D. L., Erwin, D.H., 2001. Secular Distribution of Biogenic Silica through the Phanerozoic: Comparison of Silica-Replaced Fossils and Bedded Cherts at the Series Level. The Journal of Geology, 109(4), 509-522.

Knauth, L.P., 1979. A model for the origin of chert in limestone. Geology, 7(6), 274-277.

Knauth, L.P., 1994. Petrogenesis of chert. In: Heaney, P.J., Prewitt, C.T., Gibbs, G.V. (eds.). Silica: physical behavior, geochemistry, and materials applications. Reviews in Mineralogy and Geochemistry, 29, 233-258.

Longman, M.W., 1980. Carbonate diagenetic textures from nearsurface diagenetic environments. American Association of Petroleum Geologists (AAPG) Bulletin, 64, 461-487.

Machel, H.G., 1987. Saddle dolomite as a by–product of chemical compaction and thermochemical sulfate reduction. Geology, 15, 936-940.

Macintyre, I.G., Marshall, J.F., 1988. Submarine lithification in coral reefs: same facts and misconceptions. In: Choat, J.H. (ed.). Proceedings 6th International Coral Reef Symposium. Australian Institute of Marine Science, Townsville, Australia. James Cook University Press, 263-272.

Maliva, R.G., Siever, R., 1989. Nodular chert formation in carbonate rocks. The Journal of Geology, 97, 421-433.

Maliva, R.G., 1998. Skeletal aragonite neomorphism; quantitative modelling of a two-water diagenetic system. Sedimentary Geology, 121, 179-190.

Martín-Martín, J.D., Gomez-Rivas, E., Bover-Arnal, T., Travé, A., Salas, R., Moreno-Martín-Martín, J.D., Gomez-Rivas, E., Travé, A., Salas, R., Vergés, J., 2012. Dolomías controladas por

fracturas en carbonatos aptienses de la zona de Benicàssim (SE Cuenca del Maestrat): distribución y características petrográficas. Geogaceta, 51, 19-22.

Martín-Martín, J.D., Gomez-Rivas, E., Bover-Arnal, T., Travé, A., Salas, R., Moreno-Bedmar, J.A., Tomás, S., Corbella, M., Teixell, A., Vergés, J., Stafford, S.L., 2013. The Aptian syn-rift carbonate succession of the southern Maestrat Basin (Spain): Facies architecture and fault controlled stratabound dolostones. Cretaceous Research, 41, 217-236.

Martín-Martín, J.D., Travé, A., Gomez-Rivas, E., Salas, R., Sizun, J.P., Vergés, J., Corbella, M., Stafford, S.L., Alfonso, P., 2015. Fault-controlled and stratabound dolostones in the Late Aptian-earliest Albian Benassal Formation (Maestrat Basin, E Spain): petrology and geochemistry constrains. Marine and Petroleum Geology, 65, 83-102.

Martín-Martín, J.D., Gomez Rivas, E., Gómez-Gras, D., Travé, A., Ameneiro, R., Koehn, D., Bons, P.D., 2018. Activation of stylolites as conduits for overpressured fluid flow in dolomitized platform carbonates. London, Geological Society, 459 (Special Publications), 157-176.

McGregor, H.V., Gagan, M.K., 2003. Diagenesis and geochemistry of Porites corals form Papua New Guinea: implications for paleoclimate reconstructions. Geochimica et Cosmochimica Acta, 67(12), 2147-2156.

McIntire, W.L., 1963. Trace element partition coefficients - a review of theory and applications to geology. Geochimica et Cosmochimica Acta, 27, 1209-1264.

Meyers, W.J., Lohmann, K.C., 1985. Isotope geochemistry of regionally extensive calcite cement zones and marine components in Mississippian limestones, New Mexico. In: Schneidermann, N., Harris, P.M. (eds.). Carbonate Cements. Society for Sedimentary Geology (SEPM) Special Publications, 36, 223-239.

Misik, M., 1968. Some aspects of diagenetic recristallization in limestones. XXIII International Geological Congress, 8, 129-136.

Mucci, A., 1987. Influence of temperature on the composition of magnesian calcite overgrowths precipitated from seawater. Geochimica et Cosmochimica Acta, 51, 1977-1984.

Mucci, A., Morse, J.W., 1983. The incorporation of Mg^{2+} and Sr^{2+} into calcite overgrowths: influences of growth rate and solution composition. Geochimica et Cosmochimica Acta, 47, 217-233.

Müller, A., Gagan, M.K., McCulloch, M.T., 2001. Early marine diagenesis in corals and geochemical consequences for paleoceanographic reconstructions. Geophysical Research Letters, 28(23), 4471-4474.

Perry, C.T., Hepburn, L.J., 2008. Syn-depositional alteration of coral reef framework through bioerosion, encrustation, and cementation: Taphonomic signatures of reef accretion and reef depositional events. Earth Science Reviews, 86, 106-144.

Pingitore, N.E., 1976. Vadose and phreatic diagenesis: processes, products and their recognition in corals. Journal of Sedimentary Petrology, 46, 985-1006.

Radke, B.M., Mathis, R.L., 1980. On the Formation and Occurrence of Saddle Dolomite. Journal of Sedimentary Research, 50, 1149-1168.

Ribaud-Laurenti, A., Hamelin, B., Montaggioni, L., Cardinal, D., 2001. Diagenesis and its impact on Strontium/Ca ratio in Holocene *Acropora* corals. International Journal of Earth Sciences, 90, 438-451.

Riding, R., 2011. Microbialites, stromatolites, and thrombolites. In: Reitner, J., Thiel, V. (eds.). Encyclopedia of Geobiology. Heidelberg, Encyclopedia of Earth Science Series, Springer Verlag, 635-654.

Riding, R., Tomás, S., 2006. Stromatolite reef crusts, Early Cretaceous, Spain: Bacterial origin of in situ-precipitated peloid microspar? Sedimentology, 53, 23-34.

Roca, E., Guimerà, J., 1992. The Neogene structure of the eastern Iberian margin: structural constraints on the crustal evolution of the Valencia trough (western Mediterranean). Tectonophysics, 203(1), 203-218.

Salas, J., Guimerà, J., Mas, R., Martín-Closas, A., Meléndez, A., Alonso, A., 2001. Evolution of the Mesozoic central Iberian Rift System and its Cainozoic inversion (Iberian chain). In: Ziegler, P.A., Cavazza, W., Robertson, A.H.F., Crasquin-Soleau, S. (eds.). Peri-Tethyan Memoir 6: Peri-Tethyan Rift/Wrench Basins and Passive Margins. Paris, Mémoires du Museum National d´Histoire Naturelle, 186, 145-185.

Salas, R., Casas, A., 1993. Mesozoic extensional tectonics, stratigraphy and crustal evolution during the Alpine cycle of the eastern Iberian basin. Tectonophysics, 228(1-2), 33-55.

Sayani, H.R., Cobb, K.M, Cohen, A.L., Elliott, W.C., Nurhati, I.S., Dunbar, R.B., Rose, K.A., Zaunbrecher, L.K., 2011. Effects of diagenesis on paleoclimate reconstructions from modern and young fossil corals. Geochimica et Cosmochimica Acta, 75, 6361-6373.

Sherman, C.E., Fletcher C.H., Rubin, K.H., 1999. Marine and meteoric diagenesis of Pleistocene carbonates from a nearshore submarine terrace, Oahu, Hawaii. Journal of Sedimentary Research, 69, 1083-1097.

Spötl, C., Pitman, J.K, 1998. Saddle (baroque) dolomite in carbonates and sandstones: a reappraisal of a burial-diagenetic concept. In: Morad, S. (ed.). Carbonate cementation in sandstones. International Association of Sedimentologists Special Publication, 26, 437-460.

Stoessell, R.K., Klimentidis, R.E., Prezbindowski, D.R., 1987. Dedolomitization in Na-Ca-Cl brines from 100 to 200°C at 300 bars. Geochimica et Cosmochimica Acta, 51, 847-855.

Sumner, D.Y., 1997. Late Archean calcite-microbe interactions: two morphologically distinct microbial communities that affected calcite nucleation differently. Palaios, 12, 302-318.

Sumner, D.Y., 2000. Microbial versus environmental influences on the morphology of Late Archean fenestrate microbialites. In: Riding, R., Awramik, S.M. (eds.). Microbial Sediments. Berlin, Springer Verlag, 307-314.

Swei, G.H., Tucker, M.E., 2012. Impact of diagenesis on reservoir quality in ramp carbonates: Gialo formation (Middle Eocene), Sirt Basin, Libya. Journal of Petroleum Geology, 35, 25-47.

Tomás, S., 2007. Sistemas arrecifales del Cretácico inferior de la Cuenca del Maestrat. Modelos deposicionales, paleontológicos y diagenéticos. PhD. Thesis. Barcelona, Universitat de Barcelona, 192pp.

Tomás, S., Aguirre, J., Braga, J.C., Martín-Closas, C., 2007a. Late Hauterivian coralline algae (Rhodophyta, Corallinales) from the Iberian Chain (E Spain). Taxonomy and the evolution of multisporangial reproductive structures. Facies, 53, 79-95.

Tomás, S., Comas Nebot, M., Salas, R., 2007b. La plataforma carbonatada Aptiense superior de Benicàssim-Orpesa (Cuenca del Maestrat, Cadena Ibérica): modelo de depósito. Geogaceta, 41, 235-238.

Tomás, S., Parcerisa, D., Travé, A., 2007c. Evolución diagenética de la plataforma carbonatada Aptiense superior del sector Benicàssim-Orpesa. Cuenca del Maestrat. Geogaceta, 41, 239-242.

Tomás, S., Löser, H., Salas, R., 2008. Low-light and nutrient-rich coral assemblages in an Upper Aptian carbonate platform of the southern Maestrat Basin (Iberian Chain, eastern Spain). Cretaceous Research, 29(3), 509-534.

Travé, A., Calvet, F., Sans, M., Vergés, J., Thirlwall, M., 2000. Fluid history related to the Alpine compression at the margin of the south-Pyrenean Foreland basin: the El Guix anticline. Tectonophysics, 321, 73-102.

Travé, A., Labaume, P., Calvet, F., Soler, A., 1997. Sediment dewatering and pore fluid migration along thrust faults in a foreland basin inferred from isotopic and elemental geochemical analyses (Eocene southern Pyrenees, Spain). Tectonophysics, 282, 375-398.

Veizer, J., Ala, D., Azmy, K., Bruckschen, P., Buhl, D., Bruhn, F., Carden, G.A.F., Diener, A., Ebneth, S., Godderis, Y., Jasper, T., Korte, C., Pawellek, F., Podlaha, O.G., Strauss, H., 1999. $^{87}Sr/^{86}Sr$, $\delta^{13}C$, and $\delta^{18}O$ evolution of Phanerozoic seawater. Chemical Geology, 161(1), 59-88.

Veizer, J., Hoefs, J., 1976. The nature of O^{18}/O^{16} and C^{13}/C^{12} secular trends in sedimentary carbonate rocks. Geochimica et Cosmochimica Acta, 40, 1387-1395.

Veizer, J., Holser, W.T., Wilgus, C.K., 1980. Correlation of $^{13}C/^{12}C$ and $^{34}S/^{32}S$ secular variations. Geochimica et Cosmochimica Acta, 44, 579-587.

Walker, T.R., 1960. Carbonate replacement of detrital crystalline silicate minerals as a source of authigenic silica in sedimentary rocks. Geological Society of America (GSA) Bulletin, 71(2), 145-152.

Walker, T.R., 1962. Reversible nature of chert-carbonate replacement in sedimentary rocks. Geological Society of America (GSA) Bulletin, 73(2), 237-242.

Webb, G.E., Northdurft, L.D., Kamber, B.S., Kloprogge, J.T., Zhao, J.-X., 2009. Rare earth geochemistry of scleractinian coral skeleton during meteoric diagenesis: a sequence through neomorphism of aragonite to calcite. Sedimentology, 56(5), 1433-1463.

Whittle, G.L., Alsharhan, A.S., 1994. Dolomitization and chertification of the Early Eocene Rus Formation in Abu Dhabi, United Arab Emirates. Sedimentary Geology, 92(3-4), 273-285.

Wilson, M.E.J., Ee Wah, E.C., Dorobek, S., Lunt, P., 2013. Onshore to offshore trends in carbonate sequence development, diagenesis and reservoir quality across a land-attached shelf in SE Asia. Marine and Petroleum Geology, 45, 349-376.

Yao, S., Gomez-Rivas, E., Martín-Martín, J.D., Gómez-Gras, D., Travé, A., Griera, A., Howell, J.A., 2020. Fault-controlled dolostone geometries in a transgressive–regressive sequence stratigraphic framework. Sedimentology, 67, 3290-3316.

Manuscript received January 2025;
revision accepted June 2025;
published Online September 2025.